**Figure 3.** Fixed-bearing cruciate-retaining components of the prosthetic knee prototype used in the simulation (Kyocera, Kyoto, Japan).

surface in the coronal plane was curved with a well-fitting coronal geometry for the femoral component by a curve-on-curve design (Fig. 4c). Both the high- and low-constrained designs had a high anterior lip. However, the low-constrained design is less constrained in the coronal plane, so the insert allows high rotational flexibility.
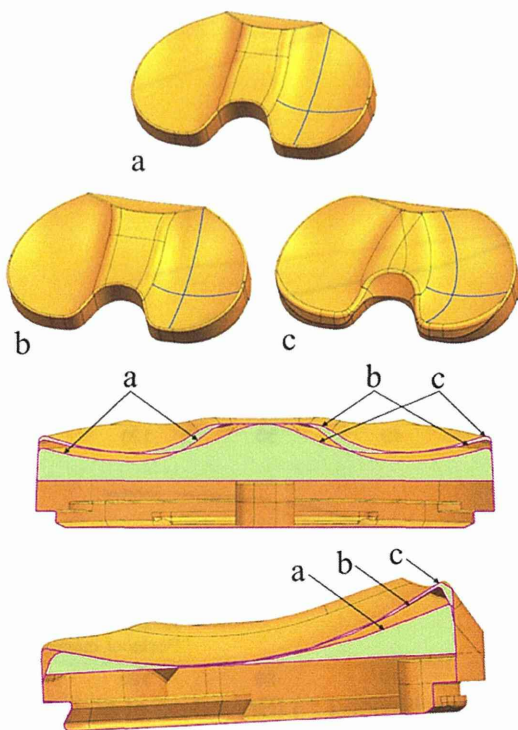
Figure 4. Three geometries of the tibial insert: (a) the standard design, (b) the high-constrained geometry with greater AP stability compared with the standard design, and (c) the low-constrained geometry with high rotational flexibility.

In aligning the components in the coronal plane, the femoral component was set perpendicular to the mechanical axis that connected the center of the knee and the center of the femoral head, and the tibial component was set perpendicular to the mechanical axis that connected the center of the knee and the center of the ankle. For the sagittal alignment, the femoral component was aligned to the distal anatomical axis of the femur, and the tibial component was aligned to the proximal anatomical axis of the tibia with 3° of posterior slope. The neutral rotational alignments of the femoral and tibial components were aligned according to the femoral epicondylar axis and the tibial anteroposterior axis, respectively.

Previous studies reported that the peak tibiofemoral contact force in normal or TKA patients during a squat increased up to 4–6 times body weight.[24–26] In the testing conditions, a constant vertical force corresponding to a body weight of 80 kg was converted into ~4,000 N (i.e., 5 times the installed weight) loading on the bicondylar joint of the knee. This was applied at the hip. The active driving elements were the quadriceps and hamstrings forces. This simulation was driven by a controlled actuator arrangement similar to a physical machine such as an Oxford-type knee rig. A closed-loop controller applied tension to the quadriceps and hamstrings to match firing to a prescribed flexion angle at each point, and cocontraction between these muscles was defined.

The z-axis (+: proximal, −: distal) of the model was defined as the extension of the tibial axis. The plane normal to the z-axis at the center of the knee was defined as the xy-plane. The x-axis (+: lateral, −: medial) was defined as the extension of the femoral epicondylar axis, which was projected onto the xy-plane along the z-axis. The y-axis (+: anterior, −: posterior) was defined as the extension of the tibial AP axis, which was perpendicular to the x-axis and was projected onto the xy-plane. The tibiofemoral and patellofemoral contact forces were a compressive joint reaction perpendicular to the tibial and patellar inserts against the femoral component. The force at the LCL comprises the traction force between the femoral and tibial attachments. The anterior and posterior bundles of the MCL were modeled with two strands, each with identical characteristics, which split the total force at the start-up position. The modeled systems were subjected to one 4.5 sec cycle of a squat (0°–130°–0° flexion).

The LCL, MCL, and PCL forces were measured in this testing condition. The tibial rotational alignments were changed between 15° external and 15° internal rotation in 5° increments, and ligament forces were compared between the malrotated conditions of the tibial component using the three constrained geometries of the insert. The rotational positions of the femur against the tibia were also measured as the angle between the femoral epicondylar axis and the tibial AP axis projected onto the xy-plane. The rotational angles (+: external, −: internal) of the femur against the tibia were calculated in the same protocol during weight-bearing deep knee flexion.
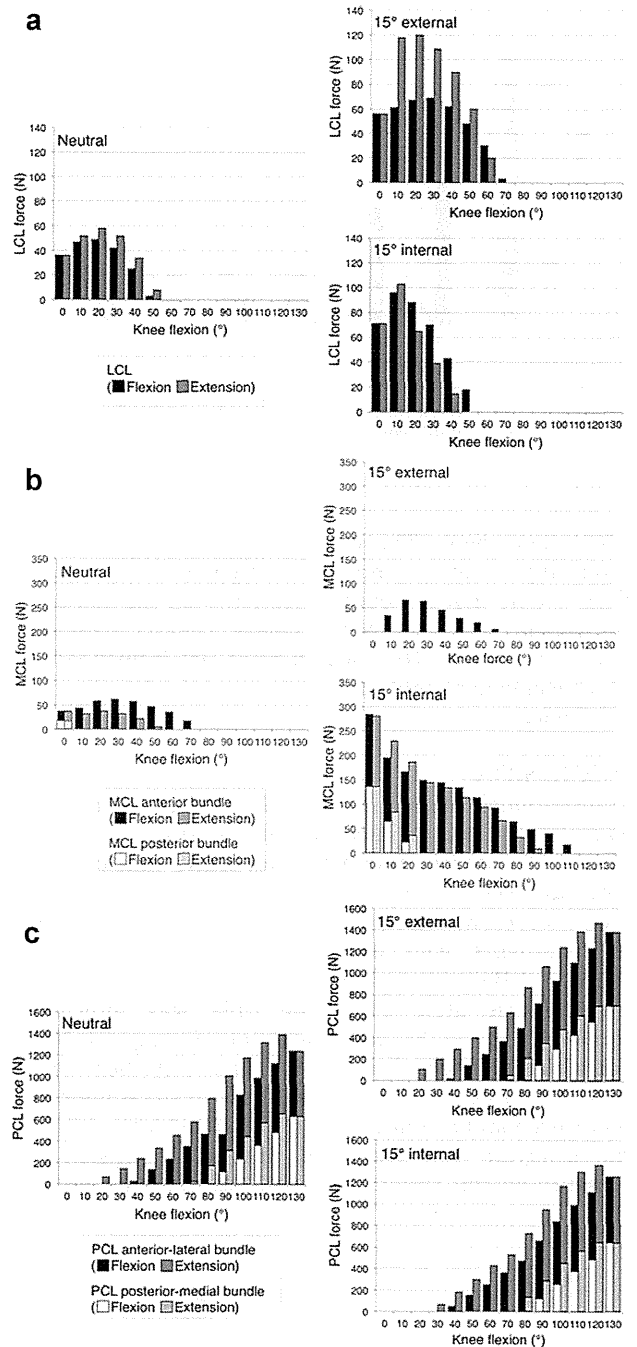
Tibiofemoral and patellofemoral contact forces were measured under the same testing conditions. Contact stresses at the patellar component and at the tibial inserts against the femoral component interfaces were calculated using 3D finite element (FE) analysis. The FE analysis study included the femoral, tibial, and patellar components. The stress states at the component interfaces were examined at 50° and 100° of knee flexion. FE simulations were performed using ANSYS Workbench version 12.0.1 (ANSYS, Inc., Canonsburg, PA).

The elastic modulus of the femoral component (Co–Cr–Mo alloy) was 240 GPa. The material property values of the tibial and patellar polyethylene components were taken from a previous study of nonlinear ultra-high molecular weight polyethylene.[27] We used the values and directions of each force at 50° flexion with 15° external and 15° internal tibial malposition computed by KneeSIM to perform the FE analysis.

RESULTS

The MCL force with the standard tibial component in the neutral position increased in early flexion, reached a peak value of 67.3 N at 27.4° flexion, and then decreased gradually up to 80° flexion. The LCL, MCL, and PCL forces with the neutral, 15° internal, and external conditions of the tibial component using the standard insert during weight-bearing deep knee flexion were calculated (Fig. 5). The peak MCL forces of the anterior and posterior bundles were 67.3 N (27.4°) and 18.7 N (0°), respectively, under neutral conditions. With internal rotation of the standard component, the peak MCL forces increased progressively up to 285.2 N. By contrast, with external rotation of the standard component, the peak MCL forces increased only a small amount. The MCL forces with the high-constrained and low-constrained components in neutral tibial rotation were almost identical to those with the standard component. In the condition of 15° internal rotation of the tibia, the high-constrained component caused an increase of ~15%, and the low-constrained component caused a decrease of ~15% in the peak MCL force compared with the standard component (Fig. 6). In 15° external tibial rotation, the MCL forces were about the same (70 N) in the three geometries.

The LCL force with the standard tibial component in neutral rotation had a peak value of 58.1 N at 18.8° flexion, and this declined up to 50° flexion. With internal and external rotation of the standard component, the LCL peak forces increased slightly to 113.4 N and 120.1 N, respectively (Fig. 7). The LCL forces with the high-constrained and low-constrained components in neutral tibial rotation did not differ greatly from those of the standard component. For 15° of internal tibial rotation, the high-constrained component had almost the same LCL forces as the standard component, but the peak LCL force in the low-constrained component was ~30% less than that of the standard component. The rotational position of the femur against the tibia during flexion was affected by the rotational alignment of the tibial component (Fig. 8). With internal rotation of the component, the femur tended to be internally rotated, but the degree of femoral rotation was less than half the rotational change of the tibial component. With external rotation of the tibial component, the opposite movement was found. A higher degree of constraint of the tibial component was associated with greater rotational movement of the femur. The PCL forces were hardly affected by the three different geometries of the malrotated tibial insert (Table 1).

Figure 5. LCL (a), MCL (b), and PCL (c) forces with the neutral, 15° internal, and external conditions of the tibial component using the standard insert during weight-bearing deep knee flexion.

Tibiofemoral and patellofemoral contact forces were not influenced by the malrotation and geometries of the tibial component (Fig. 9, Table 2). However, tibiofemoral contact stresses were higher in the malrotated tibial component than in the neutral position at 50° and 100° of flexion (Fig. 10). Patellofemoral contact stresses at 50° flexion also increased in the malrotated
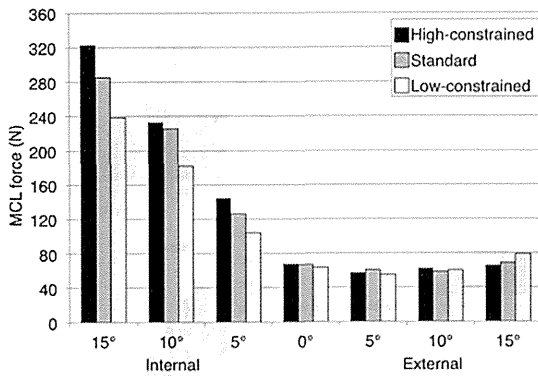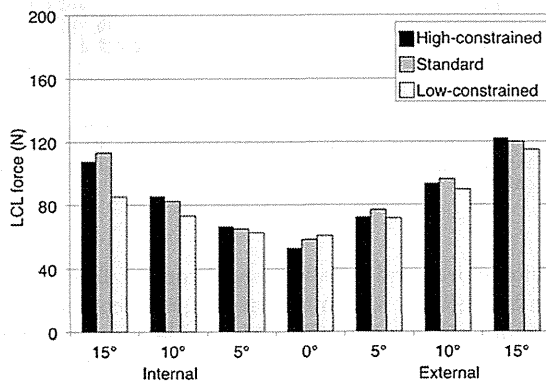
Figure 6. MCL peak forces throughout the range of motion for the malrotated tibial conditions with the three tibial insert geometries.

Figure 8. The mean, minimum, and maximum values of the rotational angles (+: external, −: internal) of the femur against the tibia during deep knee flexion with malrotation of the three tibial insert geometries.
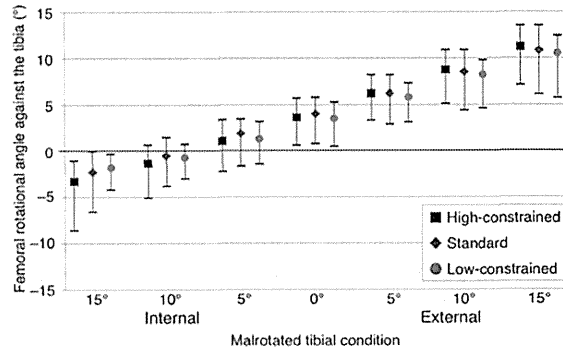
tibial component. The contact stresses with the 15° internally rotated standard component were more than double that in neutral rotation with the standard component (Fig. 11). Nevertheless, contact patellofemoral stresses at 100° flexion were not influenced by tibial component malrotation compared with those at 50° flexion.

DISCUSSION

Malrotational alignment of the tibial component causes persistent clinical problems after TKA.[5–7,28] Using CT analysis, Barrack et al. found that patients with anterior knee pain after TKA had a higher incidence of internal tibial rotation (6.2°) compared with patients who were pain free (0.4° external rotation).[1] Bédard et al. found that in patients reporting stiffness after TKA, the tibia was internally rotated in 33 of 34 cases with an average of 13.7° pathological internal rotation.[3] These studies noted that the reasons for pain or stiffness in tibial malposition were patellar maltracking, restricted lateral femoral condylar rollback, and increased tension or pressure on soft tissue; however, the influence on the

Figure 7. LCL peak forces throughout the range of motion for the malrotated tibial conditions with the three tibial insert geometries.

soft tissue was not evaluated. Consequently, we used computer simulation to analyze LCL and MCL forces and the intercomponent kinematics and kinetics in the malrotated tibial condition.

We showed that the MCL force increased significantly with internal rotation of the tibial component. We supposed that the increased MCL tension is one of the principle causes of the painful or stiff knee in an internally rotated tibia. By contrast, the MCL peak forces with external rotation of the standard tibial geometry increased by only a small amount. The reason for this discrepancy might derive from the orientation of the MCL. MRI studies showed that the tibial attachment of the MCL is located more anteriorly relative to the femoral attachment in knee extension.[17,18] With an internally rotated tibial component, the femur is rotated internally relative to the tibia, resulting in posterior movement of the femoral medial condyle. In this situation, tensile force at the MCL is likely to increase by lengthening the distance between the ligamentous attachments. Conversely, with an externally rotated tibial component, the medial femoral condyle moves anteriorly, and the MCL length is shortened slightly or unchanged. This condition would not change the MCL force significantly. The high-constrained component had ~15% greater MCL force than the standard component with a 15° internally rotated tibial component. The kinematic analysis showed that the high-constrained component caused a greater rotational mismatch between femur and tibia than did the standard component. This caused more movement of the femur, which caused a greater increase in MCL forces. The LCL was likely influenced less in the malrotated tibial condition than the MCL because its stiffness value was smaller, and it was modelled as a single bundle compared with the MCL with two parallel bundles. Also, because the LCL orientation was almost straight in the craniocaudal direction compared with the oblique orientation of the MCL, the LCL length was not changed much by tibial component malrotation.

Table 1. Posterior Cruciate Ligament (PCL) Forces in the Malrotated Tibia with the Three Different Insert Geometries

Geometry	Internal Rotation				External Rotation		
	15°	10°	5°	0°	5°	10°	15°
PCL force (N)							
High-constrained	1093	1789	1377	1390	1417	1432	1456
Standard	1364	1385	1400	1407	1424	1429	1442
Low-constrained	1362	1769	1371	1385	1409	1417	1459
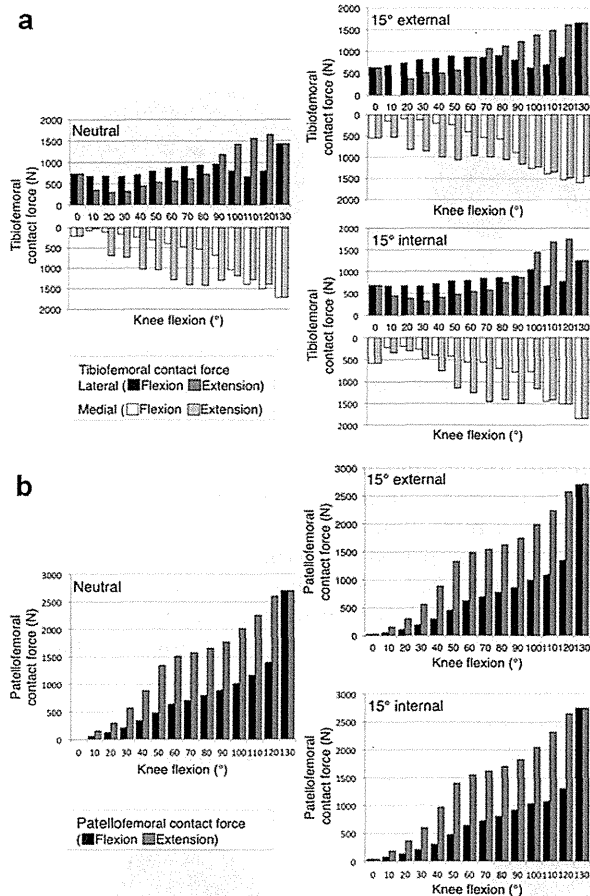
Figure 9. Tibiofemoral (a) and patellofemoral (b) contact forces with the neutral, 15° internal, and external conditions of the tibial component using the standard insert during weight-bearing deep knee flexion.

Tibiofemoral and patellofemoral contact forces were not influenced by all tibial conditions, but contact stresses increased with tibial component malrotation. Patellofemoral contact stresses with a malrotated component, especially the high-constrained geometry, were greater than those in the neutral position. Because the rotational position of the femoral component was affected by the malrotated tibial component, the patellar component maltracked, and edge loading occurred against the groove of the femoral component. We selected 50° flexion because that is the angle at which the patellofemoral contact pressure increases gradually, and this angle was in previous studies of activities such as gait and stair climbing.[29-31] We also compared the FE analysis at 100° flexion with that at 50° flexion as a quasi-static analysis. The patellofemoral contact stresses at 100° were not influenced by tibial component malrotation compared with those at 50° because the patellar component fit closely with the patellar groove of the femoral component at 100°. Although we found high values of contact stress, our results were based on dynamic forces during a deep knee bend. These results suggest that proper tibial component rotational alignment is essential for avoiding high tibiofemoral and patellofemoral joints contact stresses, which increase the risk of excessive polyethylene wear or breakage.

Previous studies reported that the maximum quadriceps force in flexion increases up to 3.5 times body weight.[32,33] In the studies by Sharma et al., the quadriceps force in flexion was similar to the patellofemoral contact forces. The peak quadriceps force was 3156 N (i.e., 4 times the installed weight) in a neutral position and was similar to the patellofemoral contact

Table 2. Tibiofemoral and Patellofemoral Contact Forces at the Component Interfaces in the Malrotated Tibia with the Three Different Insert Geometries

| Contact Force	Geometry	Internal Rotation				External Rotation		
		15°	10°	5°	0°	5°	10°	15°
Lateral tibiofemoral(N)	High-constrained	1766	1789	1732	1742	1724	1702	1703
	Standard	1775	1791	1733	1726	1732	1696	1700
	Low-constrained	1731	1772	1729	1726	1734	1709	1707
Medial tibiofemoral(N)	High-constrained	1863	1845	1864	1731	1663	1677	1645
	Standard	1872	1813	1853	1740	1659	1671	1658
	Low-constrained	1908	1887	1928	1911	1837	1887	1734
Patellofemoral (N)	High-constrained	2842	2811	2811	2814	2807	2821	2812
	Standard	2842	2807	2810	2809	2801	2810	2809
	Low-constrained	2825	2808	2819	2818	2819	2832	2818
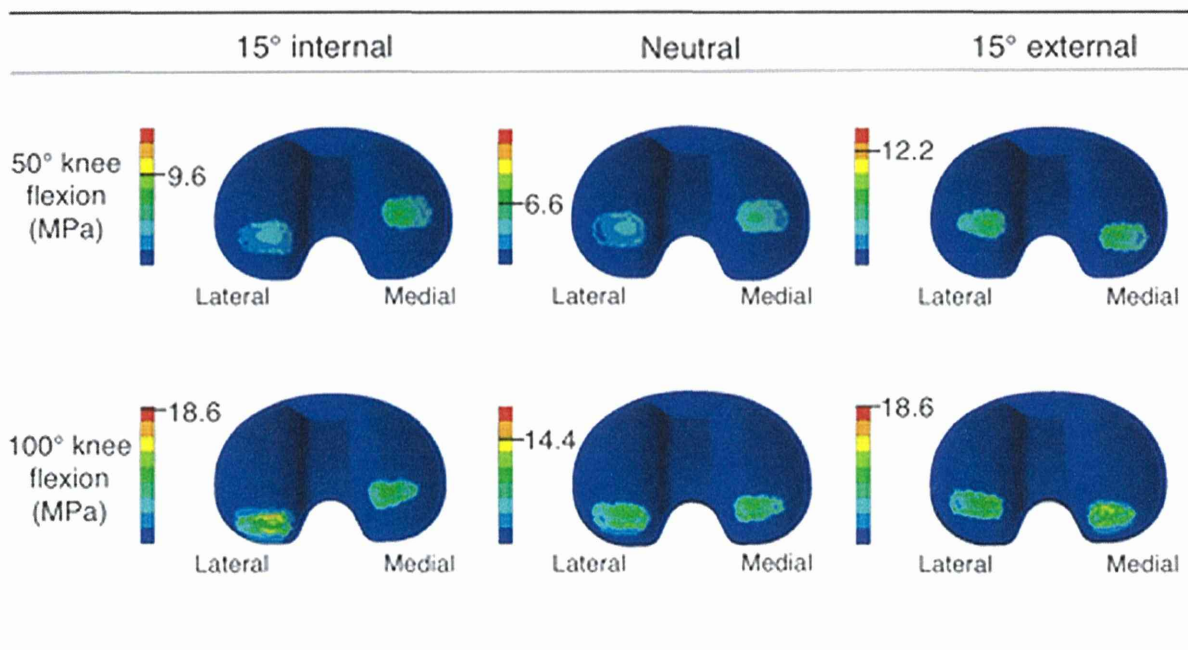
Figure 10. Tibiofemoral peak contact stresses at the component interfaces with malrotation at 50° and 100° of flexion.

forces. The force of the hamstrings was 735 N in early flexion and decreased rapidly. The tibiofemoral kinematics in our study are similar to those reported previously using fluoroscopic data.[34] In that study, Banks et al. reported that axial rotation during gait varied little between different implants and ranged from 4°–7° externally. In our study, the femur with the standard tibial component in the neutral position was rotated externally from 0.8°–5.8° with flexion (Fig. 8).

We recognize limitations to our study. First, this simulation comprised a virtual and variable model, and the material properties for soft tissues were obtained from relevant cadaveric studies. These are common methods used in most computational models,
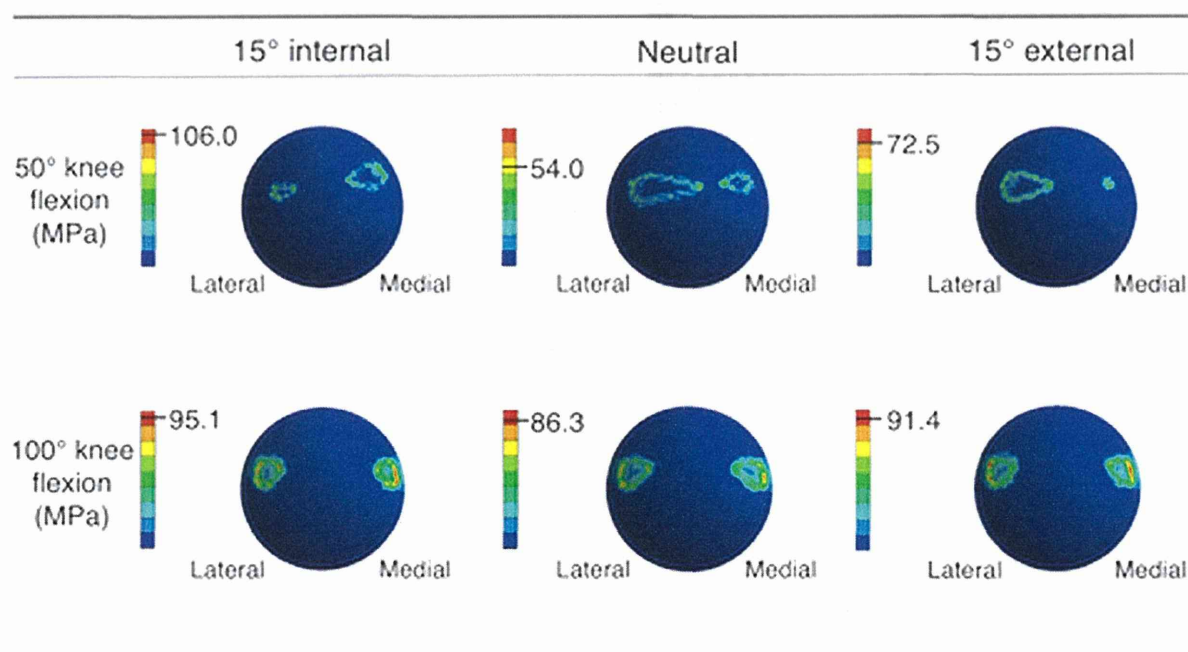
Figure 11. Patellofemoral peak contact stresses at the component interfaces with malrotation at 50° and 100° of flexion.

and we assumed the boundary conditions of each structure, muscle forces, and ankle and hip reaction forces and motions during weight-bearing deep knee flexion. However, no previous studies validated the forces of each ligament and the hamstrings during this activity. Although our force values might not be the same as in living patients, the overall trends in the changes in forces at the ligaments and articular surfaces provide useful information. Second, although we made fine adjustments to the stiffness, length patterns, and slack for each ligament from the relevant anatomical literature, our model may not have represented the simulation of TKA for varied knee deformities because of the absence of definitive data for each material property in knees with severe osteoarthritis. Third, this study included a simulation of a single attachment site location for each ligament despite the highly variable attachment site locations that occur in vivo. Finally, the prototype components and tibial geometries cannot be considered representative of all commercial fixed-bearing cruciate-retaining TKAs, and this computer simulation does not have versatility.

We measured the LCL and MCL traction forces, tibiofemoral and patellofemoral contact forces, and stresses with a malrotated tibial component in three constrained geometries during computer-simulated weight-bearing deep knee flexion. We concluded that excessive internal tibial component rotation, especially in a high-constrained geometry, increases the MCL tension and the tibiofemoral and patellofemoral contact stresses. This may explain patient complaints and polyethylene problems after TKA with a malrotated tibial component.

ACKNOWLEDGMENT

REFERENCES
1. Barrack RL, Schrader T, Bertot AJ, et al. 2001. Component rotation and anterior knee pain after total knee arthroplasty. Clin Orthop Relat Res 392:46–55.
2. Nicoll D, Rowley DI. 2010. Internal rotational error of the tibial component is a major cause of pain after total knee replacement. J Bone Joint Surg Br 92:1238–1244.
3. Bédard M, Vince KG, Redfern J, et al. 2011. Internal rotation of the tibial component is frequent in stiff total knee arthroplasty. Clin Orthop Relat Res 8:2346–2355.
4. Berger RA, Crossett LS, Jacobs JJ, et al. 1998. Malrotation causing patellofemoral complications after total knee arthroplasty. Clin Orthop Relat Res 356:144–153.
5. Matsuda S, Miura H, Nagamine R, et al. 2001. Effect of femoral and tibial component position on patellar tracking following total knee arthroplasty: 10-year follow-up of Miller–Galante I knees. Am J Knee Surg 14:152–156.
6. Merkow RL, Soudry M, Insall JN. 1985. Patellar dislocation following total knee replacement. J Bone Joint Surg Am 67: 1321–1327.
7. Wasielewski RC, Galante JO, Leighty RM, et al. 1994. Wear patterns on retrieved polyethylene tibial inserts and their relationship to technical considerations during total knee arthroplasty. Clin Orthop Relat Res 299:31–43.
8. Graw BP, Harris AH, Tripuraneni KR, et al. 2010. Rotational references for total knee arthroplasty tibial components change with level of resection. Clin Orthop Relat Res 468:2734–2738.
9. Siston RA, Goodman SB, Patel JJ, et al. 2006. The high variability of tibial rotational alignment in total knee arthroplasty. Clin Orthop Relat Res 452:65–69.
10. Chauhan SK, Scott RG, Breidahl W, et al. 2004. Computer-assisted knee arthroplasty versus a conventional jig-based technique: a randomised, prospective trial. J Bone Joint Surg Br 86:372–377.
11. Mizu-uchi H, Matsuda S, Miura H, et al. 2008. The evaluation of post-operative alignment in total knee replacement using a CT-based navigation system. J Bone Joint Surg Br 90:1025–1031.
12. Brantigan OC, Voshell AF. 1941. The mechanics of the ligaments and menisci of the knee joint. J Bone Joint Surg Am 23:44–66.
13. LaPrade RF, Bollom TS, Wentorf FA, et al. 2005. Mechanical properties of the posterolateral structures of the knee. Am J Sports Med 33:1386–1391.
14. Sugita T, Amis AA. 2001. Anatomic and biomechanical study of the lateral collateral and popliteofibular ligaments. Am J Sports Med 29:466–472.
15. Warren LF, Marshall JL, Girgis F. 1974. The prime static stabilizer of the medial side of the knee. J Bone Joint Surg Am 56:665–674.
16. Blankevoort L, Kuiper JH, Huiskes R, et al. 1991. Articular contact in a three-dimensional model of the knee. J Biomech 24:1019–1031.
17. Liu F, Gadikota HR, Kozánek M, et al. 2011. In vivo length patterns of the medial collateral ligament during the stance phase of gait. Knee Surg Sports Traumatol Arthrosc 19: 719–727.
18. Park SE, DeFrate FE, Suggs JF, et al. 2005. The change in length of the medial and lateral collateral ligaments during in vivo knee flexion. Knee 12:377–382.
19. Wijdicks CA, Ewart DT, Nuckley DJ, et al. 2010. Structural properties of the primary medial knee ligament. Am J Sports Med 38:1638–1646.
20. Edwards A, Bull AM, Amis AA. 2007. The attachments of the fiber bundles of the posterior cruciate ligament: an anatomic study. Arthroscopy 23:284–290.
21. Harner CD, Xerogeanes JW, Livesay GA, et al. 1995. The human posterior cruciate ligament complex: an interdisciplinary study. Ligament morphology and biomechanical evaluation. Am J Sports Med 23:736–745.
22. Robinson JR, Bull AM, Amis AA. 2005. Structural properties of the medial collateral ligament complex of the human knee. J Biomech 38:1067–1074.
23. Belvedere C, Ensini A, Feliciangeli A, et al. 2012. Geometrical changes of knee ligaments and patellar tendon during passive flexion. J Biomech 45:1886–1892.
24. Innocenti B, Pianigiani S, Labey L, et al. 2011. Contact forces in several TKA designs during squatting: a numerical sensitivity analysis. J Biomech 44:1573–1581.
25. Nagura T, Matsumoto H, Kiriyama Y, et al. 2006. Tibiofemoral joint contact force in deep knee flexion and its consideration in knee osteoarthritis and joint replacement. J Appl Biomech 22:305–313.
26. Smith SM, Cockburn RA, Hemmerich A, et al. 2008. Tibiofemoral joint contact forces and knee kinematics during squatting. Gait & Posture 27:376–386.
27. Kurtz SM, Muratoglu OK, Evans M, et al. 1999. Advances in the processing, sterilization, and crosslinking of ultra-high

molecular weight polyethylene for total joint arthroplasty. Biomaterials 20:1659–1688.

28. Sternheim A, Lochab J, Drexler M, et al. 2012. The benefit of revision knee arthroplasty for component malrotation after primary total knee replacement. Int Orthop 36:2473–2478.

29. Bytyqi D, Shabani B, Lustig S, et al. 2014. Gait knee kinematic alterations in medial osteoarthritis: three dimensional assessment. Int Orthop 38:1191–1198.

30. Hehne HJ. 1990. Biomechanics of the patellofemoral joint and its clinical relevance. Clin Orthop Relat Res 258:73–85.

31. Moissenet F, Chèze L, Dumas R. 2014. A 3D lower limb musculoskeletal model for simultaneous estimation of mus-culo-tendon, joint contact, ligament and bone forces during gait. J Biomech 47:50–58.

32. Sharma A, Komistek RD, Ranawat CS, et al. 2007. In vivo patellofemoral forces in high flexion total knee arthroplasty. J Arthroplasty 22:404–416.

33. Sharma A, Leszko F, Komistek RD, et al. 2008. In vivo patellofemoral forces in high flexion total knee arthroplasty. J Biomech 41:642–648.

34. Banks SA, Hodge WA, 2004. 2003 Hap Paul Award Paper of the International Society for Technology in Arthroplasty. Design and activity dependence of kinematics in fixed and mobile-bearing knee arthroplasties. J Arthroplasty 19:809–816.

KNEE

Is a "sulcus cut" technique effective for determining the level of distal femoral resection in total knee arthroplasty?

**Shinichi Kuriyama · Katsufumi Hyakuna ·
Satoshi Inoue · Yasuyuki Tanaka · Yasuyuki Tamaki ·
Hiromu Ito · Shuichi Matsuda**

Abstract

Purpose Determining the level of distal femoral resection is crucial when performing total knee arthroplasty (TKA). However, variations in distal femoral resection are encountered unexpectedly. A "sulcus cut" technique is sometimes used to determine the level of distal femoral resection, but its effectiveness has not been evaluated. The aim of this study was to examine the reliability of the sulcus cut technique using computer simulation for preoperative planning.
Methods This study group comprised 40 knees in 34 patients (22 women, 12 men) scheduled for TKA. The preoperative planning software of a computed tomography (CT)-based navigation system was used. We determined the resected level of the femur so that the bone–implant interface of the femoral component was adjusted to the deepest subchondral bone of the trochlear groove in coronal CT images. We then measured each perpendicular distance from the resected surface of the proximal femur to the most distal point of the lateral and medial femoral condyles.
Results The mean distances of the distal–lateral and distal–medial condylar resections from the femoral sulcus were 7 mm (±1 mm) and 8 mm (±1 mm), respectively. The resection level did not differ significantly between men and women or between different component sizes. There was a slightly positive correlation between the femoral mechanical and anatomical axis angle and the distance

of the distal–lateral condylar resection from the femoral sulcus.
Conclusions The sulcus cut technique can be used to determine the desirable level of the distal femoral resection in TKA.
Level of evidence Case series, Level IV.

Keywords Total knee arthroplasty · Femoral sulcus · Distal femoral resection · Joint line · Computer simulation

Introduction

Determining the level of distal femoral resection is very important in total knee arthroplasty (TKA). At the desirable level of distal femoral resection, the original joint line is restored, and thus, the balance is maintained between the soft tissues during knee extension [12, 26, 28]. This is important because tight ligaments caused by insufficient resection can lead to extension contracture [8, 22, 35] and excessive wear of the ultra-high molecular weight polyethylene of the tibial component [20, 36]. Alternatively, elevation of the joint line because of excessive resection may result in mid-flexion instability [22, 27] and anterior knee pain associated with increased patellofemoral loading [18] and patellar crepitus [14].

We sometimes encounter variations in distal femoral resection using a distal femoral cutting block because of pathological conditions in the distal articular surfaces [24, 25, 30]. A previous study reported that the distal and posterior parts of the lateral condyle appeared to be distorted in magnetic resonance imaging analysis, especially when applied to a valgus knee [23]. It is difficult to determine the level of distal resection from the lateral or medial distal joint surface of the femur in cases with severe femoral

S. Kuriyama (✉) · H. Ito · S. Matsuda
Department of Orthopaedic Surgery, Graduate School
of Medicine, Kyoto University, 54 Kawahara-cho, Shogoin,
Sakyo-ku, Kyoto 606-8507, Japan
e-mail: kuriyama@kuhp.kyoto-u.ac.jp

K. Hyakuna · S. Inoue · Y. Tanaka · Y. Tamaki
Department of Orthopaedic Surgery, Japanese Red Cross Society
Wakayama Medical Center, Wakayama, Japan
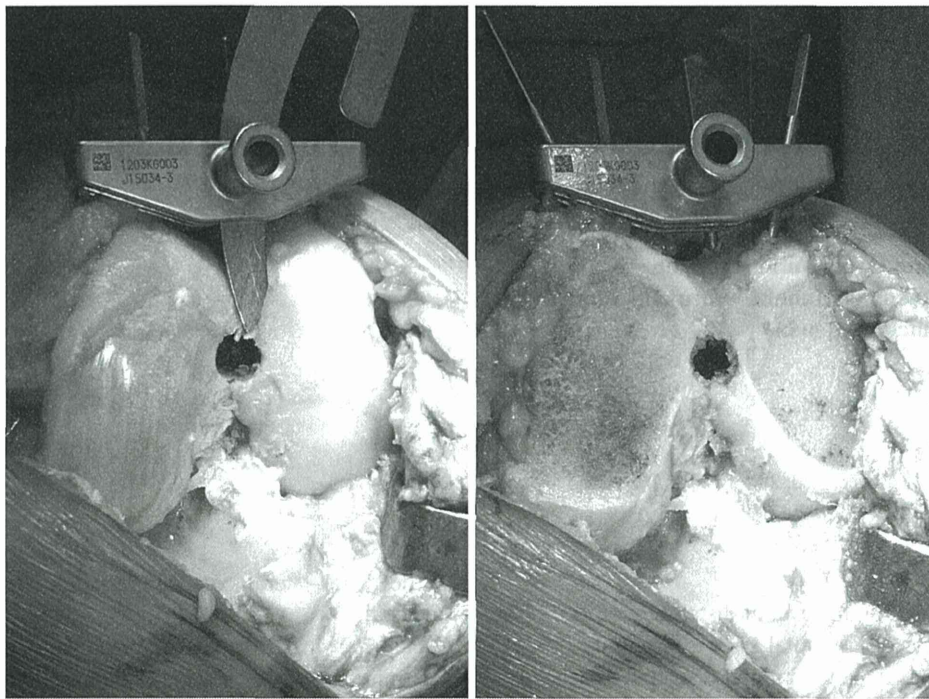
Fig. 1 Sulcus cut technique used to determine the level of distal femoral resection from the deepest portion of the trochlear groove with the stylus, creating a butterfly pattern on the cutting surface

articular deformity with or without the use of a navigation system [17].

Additional bone resection of the distal femur is troublesome after preparation of the chamfer cut. Previous studies have reported methods to determine the original joint line using the ratio of the transepicondylar width of the femur and the perpendicular distance from the epicondyles to the joint line tangent [13, 16, 31, 33]. These methods are useful in revision TKA, but are too complex for primary TKA because the distance of bone resected needs to be calculated intraoperatively. A simpler method using the "sulcus cut" technique, in which the distal cutting level is adjusted to the sulcus of the distal femur, is used clinically to determine the level of distal femoral resection (Fig. 1). The femoral sulcus has been used for rotational alignment [2] and as a mediolateral landmark [10, 21]. However, the femoral sulcus has never been evaluated as an index for determining the level of distal femoral resection. We hypothesized that the sulcus cut technique would have high clinical reliability for determining the desirable level of the distal femoral resection.

The current study examined the precision and effectiveness of the sulcus cut technique using computer simulation software for preoperative planning. The influences of sex, component size, and the femoral mechanical and anatomical axis (FMA) angle on the effectiveness of the sulcus cut technique were also evaluated.

Materials and methods

The study group comprised 40 knees in 34 Japanese patients (22 women, 12 men) who were scheduled to receive TKA from 2006 to 2008. The preoperative diagnosis was varus osteoarthritis in all knees, and the mean age of the patients at the time of diagnosis was 75.1 years (range 64–85 years). All patients had a completely defective medial joint space of the knee on preoperative standing anteroposterior radiographs. All patients provided informed consent for these operative procedures and risk of radiation exposure. The patients were assessed using computed tomography (CT) scans for preoperative planning.

The preoperative planning software of the CT-based navigation system (Vector Vision Knee 1.6; Brainlab Inc., Heimstetten, Germany) was used. The Bi-Surface knee system (Kyocera Medical, Osaka, Japan) was used as a digital template of the femoral component with cruciate-substituting design for preoperative measurement. The distal thickness of the femoral component was 8.5 mm, and the anteroposterior dimensions of the standard, large, and extra-large femoral components were 57.3, 60.3, and 63.5 mm, respectively. For the CT scans, the femoral head, knee joint, and ankle joint without the femoral shaft and tibial shaft were scanned with a slice thickness of 2 mm in immediate succession.
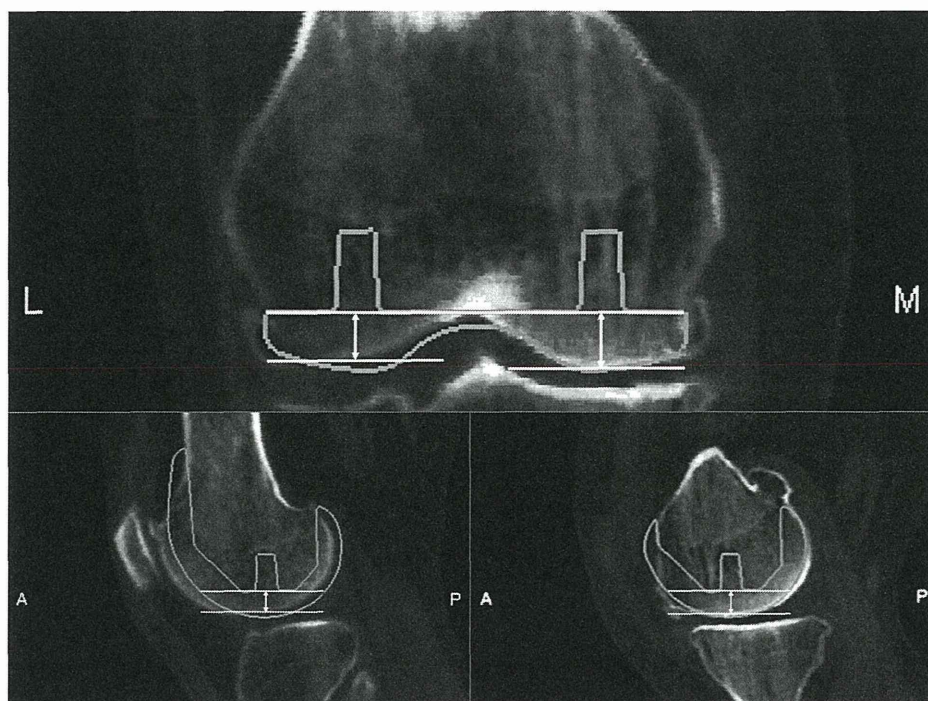
Fig. 2 Fitting of the digital template of the femoral component to the deepest portion of the trochlear groove using preoperative planning software. The distance from the planned resection line to the most distal part of the medial and lateral femoral condyles was measured

To align the components in the coronal plane, the femoral component was set perpendicular to the mechanical axis that connected the center of the knee and the center of the femoral head. For the sagittal alignment, the femoral component was aligned to the anatomical axis that connected the center of the lateral knee and the center of the femoral shaft. The neutral rotational alignment of the femoral component was determined according to the surgical epicondylar axis, which is a line connecting the sulcus of the medial epicondyle and the most prominent point of the lateral epicondyle of the femur [9, 11]. The anatomical axis was then defined as a straight line that connected the mid-diaphyseal path of the femur and the center of the knee. The preoperative planning software to determine the FMA angle, which was defined as the angle between the femoral mechanical and anatomical axes, was used. To obtain the measurements using the preoperative planning software, we first selected a suitably sized femoral component using the anterior–posterior dimension for each patient and aligned the femoral component perpendicular to the coronal mechanical and sagittal anatomical axes.

In the sulcus cut technique, the distal femoral cutting block is first aligned to the planned axis (mechanical axis of the femur). Next, the deepest portion of the trochlear groove is checked with a stylus, and the resected level of the distal femoral cutting block is adjusted so that the distal

bone–implant interface of the femoral component is identical to the deepest subchondral bone of the trochlear groove. Finally, the distal femur is cut by creating a butterfly pattern on the cutting surface, as shown in Fig. 1. Therefore, in this simulation study, we determined the resected level of the femur strictly, so that the distal bone–implant interface of the femoral component was identical to the deepest subchondral bone of the trochlear groove in the coronal CT images using the preoperative planning software (Fig. 2). The perpendicular distances from the resected line to the most distal points of the lateral and medial femoral condyles were measured using a digital template in 1 mm increments. The same examiner performed all measurements throughout this study. This study was approved by the Institutional Review Board of the Red Cross Society Wakayama Medical Center (registration number 298).

Statistical analysis

Differences between the measured distances were analyzed using the nonparametric Mann–Whitney U test for independent samples. The significance level was set at 5 %. This sample size was chosen from the data reported by similar previous studies [6, 10, 15] and was calculated using a power analysis [6]. The sample size with 80 % power ($\alpha = 0.05$) indicated a minimum sample size of 24